Hindawi
Advances in Materials Science and Engineering
Volume 2020, Article ID 6562373, 11 pages
https://doi.org/10.1155/2020/6562373

Research Article

Curing Temperature Effects on the Tensile Properties and Hardness of $\gamma - Fe_2O_3$ Reinforced PDMS Nanocomposites

Yvonne Konku-Asase,[1] **Abu Yaya**,[2] **and Kwabena Kan-Dapaah**[1]

[1]*Department of Biomedical Engineering, School of Engineering Sciences, P.O. Box LG 77, Legon, Ghana*
[2]*Department of Materials Science and Engineering, School of Engineering Sciences, P.O. Box LG 77, Legon, Ghana*

Correspondence should be addressed to Kwabena Kan-Dapaah; kkan-dapaah@ug.edu.gh

Received 1 May 2020; Revised 21 June 2020; Accepted 23 June 2020; Published 16 July 2020

Academic Editor: Stefano Bellucci

The mechanical properties of plain polydimethylsiloxane (PDMS) and its nanocomposites have been exploited for various theranostic biomedical applications. Although several research groups have investigated the effects of preparation conditions—especially curing temperature and time—on bulk mechanical properties of plain PDMS, there are no reported similar studies for its nanocomposites. In this study, mechanical properties of PDMS reinforced by different volume fractions (ϕ_{mnp} = 0–2 vol. %) of γ-Fe_2O_3 nanoparticles (NPs) were investigated and quantitative data presented for different curing temperatures (25, 100, and 150°C). To a large extent, γ-Fe_2O_3 NPs were uniformly dispersed in the PDMS matrix with no primary chemical bonds formed. For the temperatures tested, the data showed an increase for Young's modulus (E) of about 170% (1.36–3.71 MPa) and a decrease of the ultimate tensile strength (UTS) of about 65% (6.48–2.93 MPa) with increasing concentration of the NPs. Furthermore, hardness (Shore A) (H) increased with curing temperature but decreased with concentration. Based on the findings, we conclude that the linear relationship between the calculated mechanical properties (E, UTS, H) and small ϕ_{mnp} is independent of the curing temperature. The experimental data provide useful background information for the selection of processing parameters for PDMS nanocomposite fabrication.

1. Introduction

Polydimethylsiloxane (PDMS) is a silicone-based organic elastomer composed of a repeating $n - C_2H_6OSi - n$ unit [1]. It has a glass transition temperature below −120°C and possesses an attractive combination of properties including inertness, nontoxicity, nonflammability, biocompatibility, optical transparency, and high elasticity [2–4]. Usually, PDMS comes as a two-part kit consisting of a prepolymer (monomer) and curing agent (cross-linker) that are combined in a 10 : 1 ratio during preparation [1]. The principal steps involved in the preparation of PDMS include (a) stirring of the monomer and cross-linker mixture for homogeneity, (b) degassing with vacuum pumps or centrifuges to remove bubbles, and (c) curing at different temperatures and times using ovens [1]. It can be prepared with a wide range of relatively easy techniques such as soft lithography and its derivatives, molding, dip casting, spin coating, and 3D printing [5–8]. Notably, the ability of PDMS to undergo relatively large elastic deformation has been exploited for the development of several theranostic biomedical applications such as lab/tissue/organs-on-chip devices, point-of-care devices, and two/three-dimensional cell culture [3, 4, 9]. Examples include micropumps employing elastomeric displacement amplification [10, 11], cell-based biochips using elastomeric substrates [12, 13], and microfluidic channel for pressure monitoring [14, 15].

An increasing number of investigators have studied methods of customizing the elasticity of PDMS for different applications. Popular methods have focused on manipulating preparation and addition of relatively small amount of small particles. For the case of the former, parameters such as the monomer to cross-linker ratio as well as the curing temperature and time have been manipulated to alter the

mechanical properties of PDMS. Liu and coworkers [16] investigated the influences of curing temperature (100, 150, 200, and 300°C) and time (between 30 min and 3 h) on Young's modulus and ultimate tensile strength and reported that they increased with temperature up to 200°C and then decreased. They attributed the reduction to thermal decomposition. Johnston et al. [17] found that the compressive and tensile Young's modulus and the hardness (Shore A) increased by about 58% (117.8 to 186.9 MPa), 125% (1.32 to 2.97 MPa), and 22% (44 to 54 Sh_A), respectively, in the range of up to 40% strain when temperature was increased from 25 to 200°C. Campeau et al. [18] studied the effects of curing temperatures (50, 80, 100, and 150°C) and sterilization techniques (UV, ethanol, and boiling water) on material properties of PDMS scaffold used in endothelial mechanobiological studies. Their results showed, amongst others, that there were significant differences in Young's modulus for the range of curing temperatures tested. Furthermore, they showed that sterilization by boiling affected the mechanical properties.

The use of relatively small amounts of nanoparticles (NPs) fillers—any matter with dimensions between 1 and 100 nm [19]—to influence the mechanical properties of elastomers matrix such as PDMS has been known for decades. Notably, the incorporation of the NPs is known to increase stiffness, introduce the Mullins effect (an alteration of stiffness dependence on strain history), and change transient material behavior (e.g., stress relaxation and hysteresis). The mechanical properties of elastomeric nanocomposites have been attributed to how the fillers interact with the matrix as well as themselves: the former (filler-matrix interactions) has been shown to enhance the mechanical properties, whereas the latter (filler-filler interactions)—controlled by van der Waals and electrostatic forces—deteriorates them [20, 21], which has been mainly attributed to the difficulty to uniformly disperse NPs within a polymer matrix due to their high surface area to volume ratio and the hydrophobicity of elastomeric polymer matrices. Several theoretical models are available to correlate mechanical properties such as Young's modulus and tensile strength with the volume fraction of nanoparticles [21–24]. The resulting composite material, so-called nanocomposite, has contributed significantly to the development of smart and novel applications in several fields of biomedical engineering including biosensing, thermotherapy, single molecule analysis, cell culturing, and biomimetics [25–28] due to their low cost, high strength, and simple manufacturing processes.

In recent years, magnetic ceramics-based NPs such as magnetite (Fe_3O_4) and maghemite (γ-Fe_2O_3) have attracted a lot of interest in the fields of biomedical engineering because they exhibit exciting properties such as high electrical resistivity, ease of synthesis, resistance to corrosion/wear, high stiffness, and biocompatibility [29–31]. The combination of these magnetic NPs with elastomeric polymers such as PDMS results in the formation of stimuli responsive magnetorheological nanocomposites. The possibility of manipulating the mechanical properties of these materials under the influence of magnetic fields is of interest in the field of biomedical engineering due to the opportunity it offers for the development of novel stimuli responsive and efficient biomedical engineering systems [32–34]. For instance, Kitano et al. exploited the alternating magnetic field-controlled variable stiffness of a magnetorheological composite based on carbonyl iron particles and the polymer glycerol to develop a multijoint manipulator for laparoscopic surgery [33]. Antonel et al. showed that anisotropic properties were induced when $CoFe_2O_4$-PDMS composites were cured in the presence of an alternating magnetic field [34]. Furthermore, they reported a 4-point increase in Young's moduli along the direction parallel to the needles. Over the past few years, our group has been investigating the development of maghemite (γ-Fe_2O_3) NPs reinforced PDMS nanocomposite for the development of implantable devices for interstitial thermotherapy of tumors [35–37].

Although several investigators have separately studied the effects of curing temperature or nanoparticle concentration on the mechanical properties of PDMS under different preparation conditions, to the best of our knowledge, there has been no reported investigation of the effects of standard curing temperature conditions on bulk mechanical properties of PDMS nanocomposites. In this study, we investigated and presented quantitative data of the relationship between the bulk Young's modulus, E; ultimate tensile strength, UTS; and hardness (Shore A), H, of γ-Fe_2O_3 NPs reinforced PDMS that was prepared using soft lithography techniques and used to fabricate mechanical testing samples by a molding technique. The samples were prepared with varying volume fractions (0–2 vol. %) of the γ-Fe_2O_3 NPs and cured at three different curing temperatures (T_c) including 25, 100, and 150°C.

2. Materials and Methods

2.1. Materials. Commercially available SYLGARD 184 Silicone Elastomer kit purchased from Dow Corning Corporation (Auburn, MI, USA) and 20 nm maghemite nanoparticles (99.5% purity) from US Research Nanomaterials Inc. (Houston, TX, USA) were used to fabricate all samples.

2.2. Mold Specifications. In order to characterize the material properties of nanocomposite samples, two types of molds were manufactured in accordance with the respective American Society for Testing of Materials (ASTM) standards: ASTM D412-C and ASTM D2240-05 type A code for tensile and hardness testing, respectively.

2.3. Sample Preparation. Nanocomposite samples were prepared by varying the volume fraction of γ–Fe_2O_3 NPs within a PDMS matrix. First, PDMS matrix was prepared by mixing a prepolymer base (monomer) and cross-linking agent (hardener) at the manufacturer's recommended ratio of 10 : 1. Second, the compound was stirred for 10 min with a spatula, before adding γ–Fe_2O_3 NPs, and stirred for another 5 min to ensure uniform distribution. Third, the resulting uncured mixture was degassed using a desiccator to remove bubbles, subsequently poured into respective molds, and degassed again to eliminate any remaining bubbles. Last, the

samples were cured at temperatures recommended by Dow Corning: 25, 100, and 150°C for curing times of 48 h, 35 min, and 10 min, respectively [1]. The three types of samples that were prepared in the study were designated as MNP-0, MNP-1, and MNP-2 according to the volume fraction of nanoparticles. MNP-0, plain PDMS (γ–Fe_2O_3-free nanocomposite), was studied as a control. The sample names and their compositions are summarized in Table 1.

2.4. Structural Characterization. The crystal structure and phase purity of the γ-Fe_2O_3 NPs were substantiated using an X-ray diffractometer (D8 FOCUS X-ray, Bruker AXS Inc., Madison WI, USA). The experimental conditions used include Ni-filtered Cu-Kα radiation as the X-ray source at a power of 45 kV and 40 mA. Measurement was done at a temperature of 25°C, sampling angle of 0.08°, and 2θ scanning rate of 3 s step^{-1}. The morphology of the nanoparticles was studied with transmission electron microscope (Philips CM10, Philips Electron Optics, Eindhoven, The Netherlands). A Fourier transform infrared spectroscope (FTIR, Tensor 27, Bruker Inc., Madison WI, USA) was used to investigate the functional groups of the nanocomposite samples. A scanning electron microscope (SEM, Quanta 200 FEG MKII, FEI, Hillsboro OR, USA) was used to study the surface morphology of all samples (MNP-0, MNP-1, and MNP-2) as well as the micro distribution of the nanoparticles in the nanocomposites (MNP-1 and MNP-2). In order to prevent charging during scanning, the samples were coated with carbon. The photomicrographs were obtained at magnifications of 0.35 and 2 kx at an operating voltage of 10 kV.

2.5. Mechanical Characterization

2.5.1. Tensile Testing. Tensile testing of the samples was conducted on a Mark-10 ESM301 motorized test stand with force gauge model M5-500 (Mark-10 Corporation, Copiague, NY 11726, USA). Cross-head velocity was 25.4 cm min^{-1}. The raw data was recorded as force and time, using the MESUR Lite software version 1.3.2. Thin sheets of Teflon were inserted between the samples and grips of the machine to ensure uniform pressure distribution across the sample. Samples were tested in triplicate, and the average ambient conditions during testing were 28°C and 59% relative humidity.

The load, F (N), and time, t (s), data were transformed into engineering stress, σ_e (Pa), and strain, ϵ_e (1). σ was calculated as

$$\sigma_e = \frac{F}{A_0}, \tag{1}$$

where A_0 (m^2) is the initial cross-sectional area of the test section of the sample. ϵ_e was calculated as

$$\epsilon_e = \frac{\triangle L}{L_0}, \tag{2}$$

where $\triangle L$ (m) is the displacement and L_0 (m) is the initial length.

The stress-strain curve for all test results were plotted and fitted to a linear regression trendline in Microsoft Excel 2011 (Microsoft Corporation, Seattle, USA). According to Schneider et al. [38], Young's modulus of elastomers can be calculated via Hooke's law:

$$E = \frac{d\sigma}{d\epsilon}, \tag{3}$$

using data in the linear region, which occurs at strain levels below 40%. They also show that a geometric correction factor must be applied to accurately calculate the mechanical properties of elastomer-based materials. For the ASTM D412-C geometry used in this study, we used a correction factor of 0.50[38]. Furthermore, the UTS is calculated from the data as the stress at break point.

2.5.2. Hardness Testing. H test was performed with a Sauter HBA 100-0 Shore A Durometer (Sauter GmbH, Balingen, Germany). A force of approximately 8 N was applied, and the corresponding Shore hardness value was read on the durometer. Measurements made were repeated three times and averaged across the surface of the sample to ensure the homogeneity of data. The average ambient conditions during testing were 28°C and 59% relative humidity.

3. Results

3.1. Structural Properties. Figure 1(a) shows the X-ray diffraction spectra of the γ–Fe_2O_3 nanoparticles. The presence of peaks at $2\theta = 30.28°$, 35.72°, 43.24°, 57.24°, and 62.84° corresponding to (220), (311), (400), (511), and (440) diffraction planes confirmed the presence of γ–Fe_2O_3. The average crystallite size of the powders was determined, using Scherrer's equation [39], to be about 12.29 nm. Figure 1(b) shows the TEM image of the MNPs. The results confirmed the spherical morphology of the nanoparticles as indicated by manufacturer. The FTIR spectra defined for samples MNP-0, MNP-1, and MNP-2 are shown in Figure 1(c). The bands at A (7.56–8.64 m^{-1}), B (10.10–10.57 m^{-1}), C & D (12.57 & 14.11 m^{-1}), and E (29.50–29.62 m^{-1}) relate to $-CH_3$ rocking and Si-C stretching in $Si-CH_3$, Si-O-Si stretching, $-CH_3$ deformation in $Si-CH_3$, and asymmetric $-CH_3$ stretching in $Si-CH_3$, respectively. It is clear from the results that the characteristic peaks of plain PDMS (MNP-0) were not affected when MNPs of 1 and 2 vol. % were added to form the PDMS matrix.

Figures 1(d) to 1(i) show the fracture modes of the specimens at two different magnifications 0.35 and 2 kx. The fracture modes of sample MNP-0 were revealed to have stress waves, cracks, and wrinkles without any obvious nanoparticles (see Figures 1(d) and 1(g)). The fractured surfaces of sample MNP-1 were rougher than MNP-0 as the stress waves, cracks, and wrinkles increased with nanoparticle concentration (see Figures 1(e) and 1(h)). In addition, there was evidence of clustering of the nanoparticles and voids due to dislocation of the clusters because of the tensile load. It can be seen clearly from Figures 1(f) and 1(i) that clustering and voids increased with nanoparticle concentration.

Table 1: Composition of the samples.

No.	Sample name	Volume fraction (vol. %)	
		$[\gamma\text{–}Fe_2O_3]$ (maghemite) ϕ_{mnp}	$[n - C_2H_6OSi\text{–}n]$ (PDMS) ϕ_{pdms}
1	MNP-0	0	100
2	MNP-1	1	99
3	MNP-2	2	98

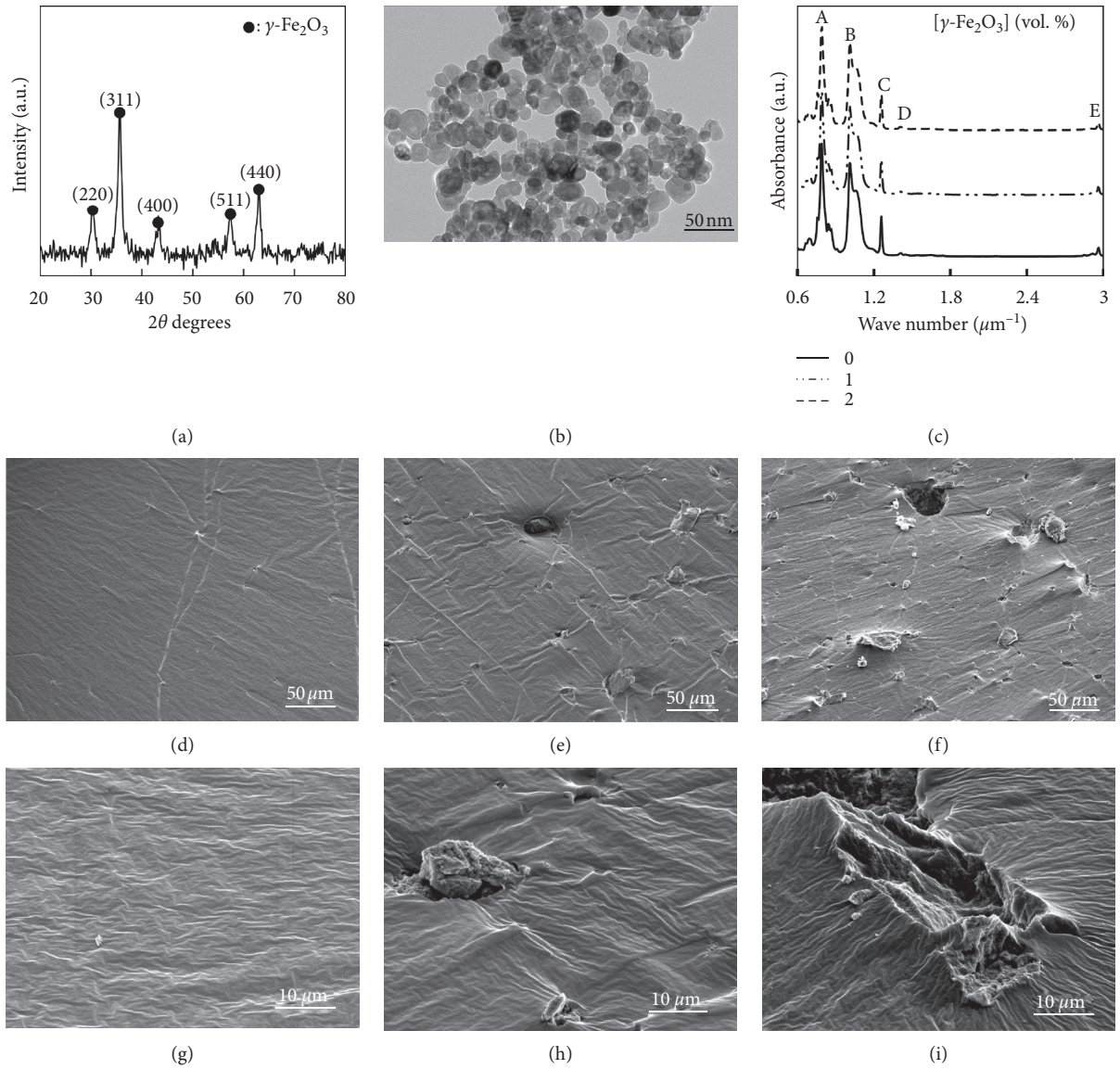

Figure 1: Structural characterization results. (a) X-ray diffraction spectra of $\gamma\text{–}Fe_2O_3$ at a power of 45 kV × 40 mA. (b) Transmission electron microscopy of $\gamma\text{–}Fe_2O_3$ at magnification of 0.5 mm, scale bar: 50 nm. (c) Fourier Transform Infrared of samples MNP-0, MNP-1, MNP-2. Fractured surfaces of samples: (d) MNP-0, (e) MNP-1, and (f) MNP-2 at a magnification of 0.35 kx and (g) MNP-0, (h) MNP-1, and (i) MNP-2 at a magnification of 2 kx. Operating voltage = 15 kV.

3.2. Mechanical Properties. The mechanical test data of the three types of samples tested were analyzed. In total, 36 samples were tested and the values were determined by averaging the triplicates. The results are summarized in Table 2 and Figures 2–4.

3.2.1. Tensile Strength

(1) Young's Modulus. The results show that E increased with T_c and ϕ_{mnp} for the samples and temperatures tested in this study (Table 2). E of MNP-0 increased by about 83% from

Table 2: Summary of the mean (± SEM), Young's modulus (E); ultimate tensile strength (UTS), and hardness (Shore A) (H) of samples MNP-0, MNP-1, and MNP-2 cured at 25, 100, and 150°C.

Sample	MNP conc. ϕ_{mnp} (vol. %)	Curing temp. T_c (°C)	Young's modulus E (MPa)	Ult. tensile strength UTS (MPa)	Hardness H (Shore A)
MNP-0	0	25	1.36 ± 0.08	6.48 ± 0.29	42.50 ± 0.73
		100	1.96 ± 0.21	5.60 ± 0.30	46.75 ± 0.61
		150	2.49 ± 0.15	4.51 ± 0.25	52.32 ± 0.55
MNP-1	1	25	1.59 ± 0.10	5.64 ± 0.24	39.67 ± 0.48
		100	2.28 ± 0.15	4.72 ± 0.40	44.83 ± 0.53
		150	3.22 ± 0.24	3.87 ± 0.18	48.88 ± 0.89
MNP-2	2	25	1.78 ± 0.37	4.88 ± 0.25	37.38 ± 0.76
		100	2.69 ± 0.14	3.84 ± 0.45	42.52 ± 0.60
		150	3.71 ± 0.35	2.93 ± 0.56	47.08 ± 0.23

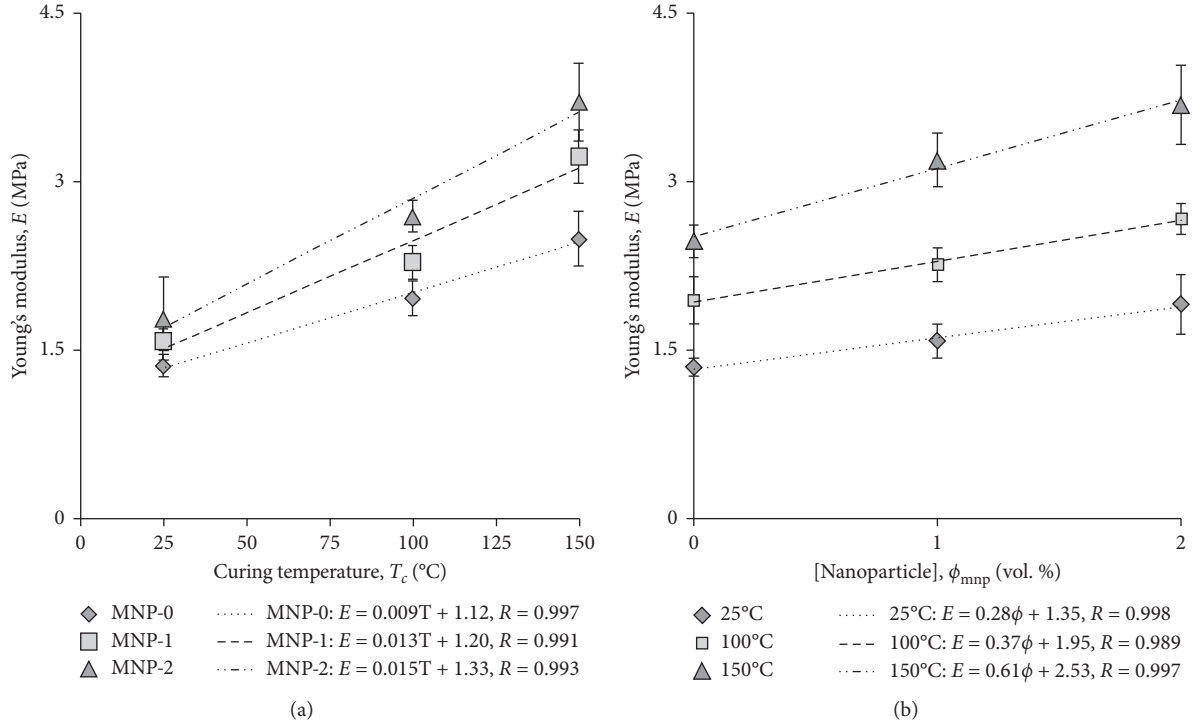

Figure 2: Young's modulus, E, as a function of (a) curing temperature, T_c, at different nanoparticle concentrations, ϕ_{mnp}, and (b) ϕ_{mnp} at different T_c.

1.36 to 2.49 MPa when T_c was increased from 25 to 150°C. For the same temperature range, E increased by 89% and 94% for samples MNP-1 (1 vol. %) and MNP-2 (2 vol. %), respectively. The rate of change of E increased by about 46% from about 0.28 to about 0.61 when T_c was increased from 25 to 150°C (Table 2). Similarly, the rate of change of E increased from ≈ 0.9 to ≈ 1.4 when ϕ_{mnp} was increased from 0 to 2 vol. % (Table 2). Finally, the linear relationships between E and the independent variables T_c and ϕ_{mnp} are depicted in Figures 3(a) and 3(b), respectively.

(2) Ultimate Tensile Strength. The results show that UTS decreased with T_c and ϕ_{mnp} for the samples and temperatures tested (Table 2). UTS of MNP-0 decreased by about 70% from 6.48 MPa to 4.51 MPa when T_c was increased from 25°C to 150°C. For the case of MNP-1 and MNP-2, UTS decreased by about 69% (from 5.64 to 3.87 MPa) and 60% (from 4.88 to 3.71 MPa), respectively, for the same change in temperature. Furthermore, it can be seen from Figure 3(a) that UTS decreased linearly with T_c for each sample. The rate of change of UTS as a function of ϕ_{mnp} slightly varied from ≈ -1 to ≈ -0.9 when T_c was increased from 25 to 150°C. The rate of change of UTS as a function of T_c varied between 0.014 and 0.020 when ϕ_{mnp} was increased from 0 to 2 vol. %. Finally, the linear relationships between UTS and the independent variables T_c and ϕ_{mnp} are depicted in Figures 3(a) and 3(b), respectively.

3.2.2. Hardness. The results show that the H increased with T_c but decreased with ϕ_{mnp} for all samples and temperatures tested in this study (Table 2). When T_c was increased from 25

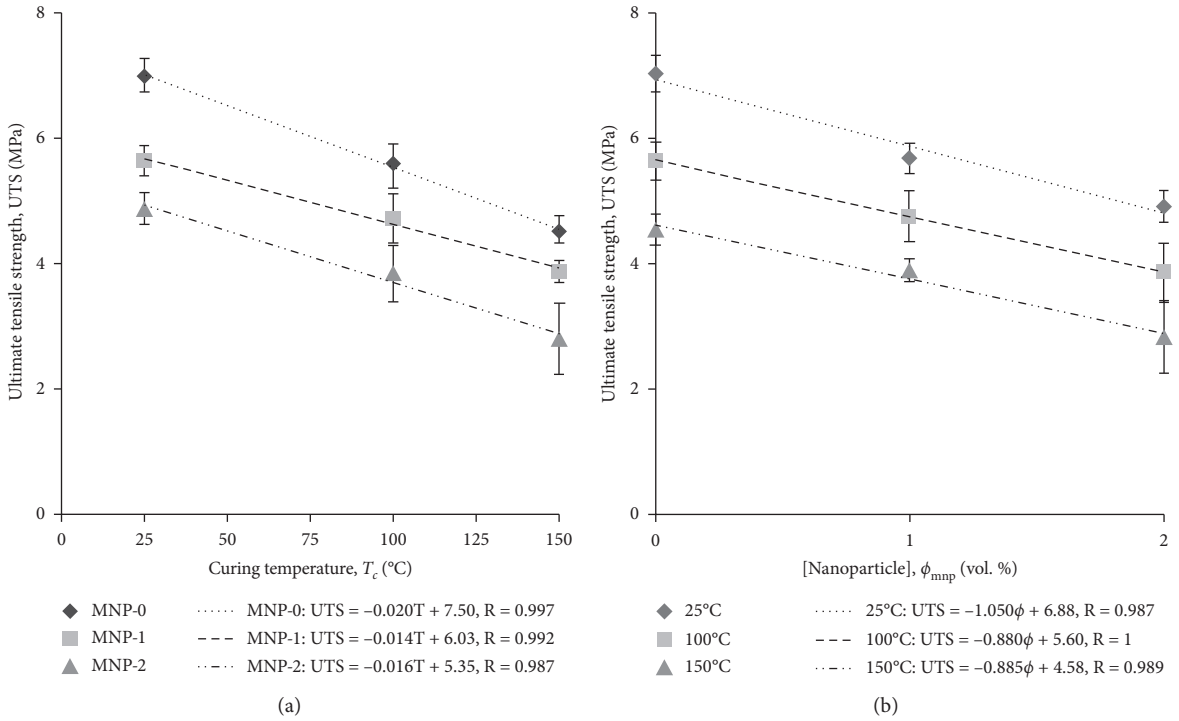

FIGURE 3: Ultimate tensile strength, UTS, as a function of (a) curing temperature, T_c, at different nanoparticle concentrations, ϕ_{mnp}, and (b) ϕ_{mnp} at different T_c.

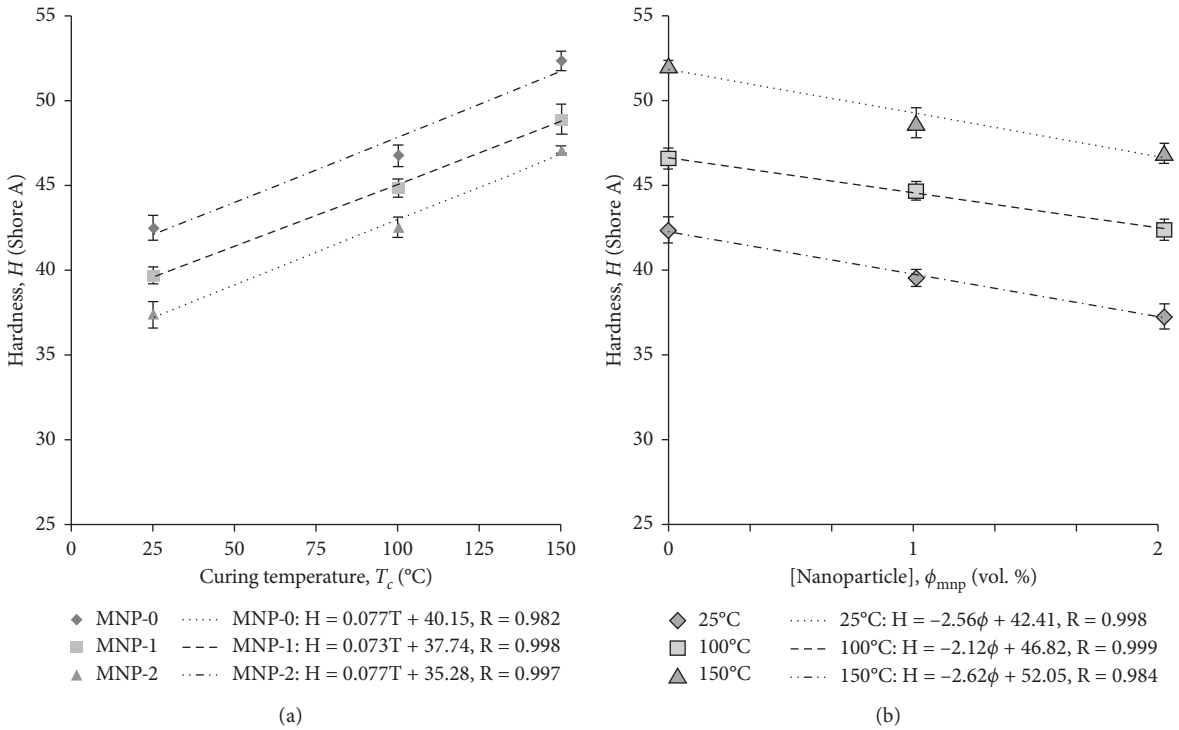

FIGURE 4: Hardness (Shore A), H, as a function of (a) curing temperature, T_c, at different nanoparticle concentrations, ϕ_{mnp}, and (b) ϕ_{mnp} at different T_c.

to 150°C, H increased between 23 and 25% for all nanocomposite samples. For the case of ϕ_{mnp}, the H decreased by about 12% from 42.50 to 37.38 when the NP content was increased from 0 (MNP-0) to 2 (MNP-2) and cured at a T_c of 25°C. At 100°C and 150°C, H decreased by about 10% and 11%, respectively, for the same samples. The rate of change

of H as a function of ϕ_{mnp} slightly varied between ≈ -2.12 to ≈ -2.62 when T_c was increased from 25°C to 150°C. The rate of change of H as a function of T_c varied between 0.073 and 0.077 when ϕ_{mnp} was increased from 0 to 2 vol. %. Finally, the linear relationships between H and the independent variables T_c and ϕ_{mnp} are depicted in Figures 4(a) and 4(b), respectively.

4. Discussion

4.1. Structural Characterization

4.1.1. FTIR. According to the FTIR results, the characteristic peaks of PDMS were maintained after the addition of the nanoparticles and were independent of the concentration. This suggests that no primary chemical bonds were formed between the nanoparticle fillers and the polymer matrix during the material preparation process.

4.1.2. SEM Micrographs. The SEM micrographs of the fractured surfaces presented in Figure 1 reveal the presence of clusters, which are dislocated under tension leaving voids on the surface. It is well known that the main factors that affect the mechanical properties of nanocomposites are the filler-matrix and filler-filler interactions [20, 21]. The former improves the mechanical properties, whereas the latter deteriorates it. The filler-filler interactions (manifested as clusters) can be attributed to factors such as the high surface area to volume ratio of nanoparticles, which makes it difficult to uniformly disperse them within a polymer matrix aiding the formation of clusters as well as their incompatibility with the hydrophobic polymer matrices due to their hydrophilicity. Although, thorough mixing can achieve uniform filler dispersion with minimal or no clusters, preprocessing techniques such as the use of saline-coupling agents [40, 41] and grafting polymers [42, 43] are sometimes used to engineer the interfacial region.

4.2. Mechanical Properties.

The mechanical measurements obtained in this study show that the mechanical behavior of γ-Fe_2O_3-PDMS nanocomposites is a function of T_c (°C) and ϕ (vol. %). Therefore, here, we discuss the results within the context of factors that affect the mechanical behavior of nanocomposites at a given temperature by comparing our results to previously reported results in the literature and theoretical models. As stated earlier, a high degree of particle-particle interaction leads to a deterioration of the performance, which is significantly improved if particle-matrix interactions are optimal.

4.2.1. Tensile

(1) Young's Modulus. Several investigators have studied the effect of processing parameters such as curing temperature and time as well as the nanoparticle concentration on Young's modulus of elastomers and their nanocomposites. Generally, these reports are similar to our results. Johnston et al. explored the effect of curing temperature on Young's modulus of plain PDMS samples manufactured by SYLGARD 184 and reported that Young's modulus of plain PDMS increased with curing temperature in the range of 25°C and 200°C[17]. Campeau and coworkers [18] found that higher curing temperatures stiffen the plain PDMS and Young's modulus varied between 1.7 and 3.7 MPa when temperature was increased within the range 50 – 150°C. Wu et al. [44] reported an elastic modulus of 1.56 MPa for plain PDMS cured at 150°C for 15 min. Also, they found that this varied between 1.71 and 2.34 MPa when weight fraction of carbon nanotubes was increased from 1.0 to 4.0.

Increasing the curing temperature of PDMS yields a more cross-linked network. Also, the bond strength of the polymerized system increases with increasing temperature due to a characteristic change from adhesive to cohesive bonding [45]. The polymerization intensity therefore increases due to increasing molecular mobility. These processes eventually result in a material with higher moduli. The lower modulus of samples that were cured at 25°C could be attributed to inconsistencies in the cross-linking process. These anomalies are associated with curing temperatures that are less than 60°C [46].

Several theoretical models are available to correlate Young's modulus with nanoparticle volume fraction in a manner similar to our results. The Guth model [23, 47] is a modified version of the model proposed by Einstein [48, 49] to estimate the relationship between Young's modulus and rigid spherical particles. It accounts for the effects of the particle-particle interaction (Figure 1), which is not considered in the Einstein model. The Guth model is defined by

$$E_G = E_m\left[1 + 0.67\phi_{mnp}g_f + 1.62\left(\phi_{mnp}g_f\right)^2\right], \quad (4)$$

where E_m is Young's modulus of the plain PDMS (sample MNP-0) and g_f is a term that is typically between 4 and 10 and accounts for the clustering effects.

Young's moduli predicted using equation (4) for lower (= 4) and upper (= 10) limits of the factor g_f are compared with the experimental values at 25°C and 150°C as shown in Figures 5(a) and 5(b), respectively. Similar to our experimental values, the predicted values increased linearly with ϕ_{mnp}. The predicted values were closer to the experimental values when $g_f = 10$ at both temperatures; however, the relative error increased with T_c and ϕ_{mnp}. For instance, at $T_c = 25$°C and $\phi_{mnp} = 1$, the relative error was about 8%; this increased to about 9% when the ϕ_{mnp} was increased to 2% at the same temperature. For the case of $T_c = 150$°C, the relative errors were estimated to be around 19% and 24%, for ϕ_{mnp} of 1 vol. % and 2 vol. %, respectively. This might be due to factors such as the influence of clustering as well as the nature of the interfacial interactions between PDMS matrix and γ–Fe_2O_3 filler.

(2) Ultimate Tensile Strength. Similar to our results, Liu and coworkers [16] studied the effects of different curing temperature on UTS and also found that the UTS decreased with curing temperature. Kan-Dapaah et al. [35] studied the UTS for the same range of nanoparticle concentration at a curing temperature of 100°C and found that the UTS decreased

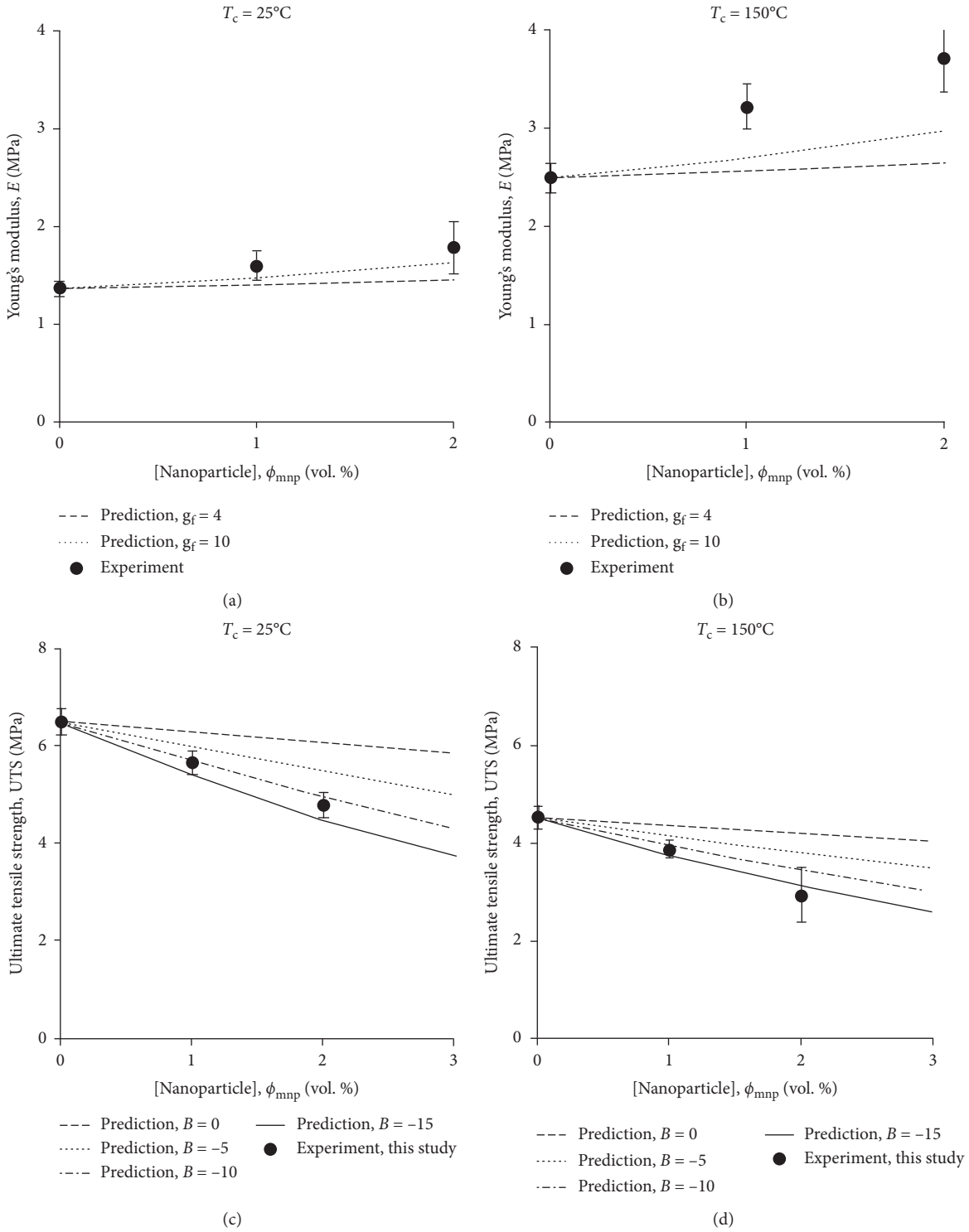

Figure 5: Predictions vs. experiments. Young's modulus (a, b) and ultimate tensile strength (c, d) as functions of the volume fraction of MNP, ϕ_{mnp}, at curing temperatures 25°C and 150°C. Dashed and dotted lines represent the theoretical values calculated using Guth model (a, b) when factor g_f is equal to 4 and 10, respectively, and Turcsanyi model (c, d) when factor B is equal to 0 and −10, respectively. Black dots represent experimental values, corresponding to samples MNP-0, MNP-1, and MNP-2 from left to right.

from 5.60 MPa to 2.41 MPa when the nanoparticle concentration increased from 0 to 10 wt.%. Based on the hypothesis that the fillers are uniformly distributed within the matrix [50, 51], the tensile strength of polymer nanocomposites has been shown to theoretically depend mainly on factors such as adhesion strength, layer thickness, and distribution profile of the fillers within the matrix. Equation (5) is a model developed by Turcsanyi et al. [24]

that relates the ultimate tensile strength to the particle concentration. The model, which assumes very strong bonding between the matrix and the fillers, is defined by

$$\mathrm{UTS_T} = \mathrm{UTS_m}\left(\frac{1-\phi}{1+2.5\phi_{\mathrm{mnp}}}\right)e^{B\phi_{\mathrm{mnp}}}. \quad (5)$$

Here $\mathrm{UTS_T}$ and $\mathrm{UTS_m}$ are the ultimate tensile strengths obtained using the Turcsanyi model and the matrix, respectively, and B is the interfacial interaction parameter, which is an empirical constant for characterizing the interfacial adhesion strength. The ultimate tensile strength, predicted with (5), as a function of ϕ_{mnp} was compared to the experimental data obtained at 25°C (Figure 5(c)) and 150°C (Figure 5(d)). The fit of (5) to the experimental data was made by varying the constant B. Similar to our results, the UTS decreased linearly with ϕ_{mnp} at both temperatures. Furthermore, at $T_c = 25$°C, the predicted values were closer to the experimental data when the constant B was −10 and −15, respectively. Again, these discrepancies between experiments and predictions can be the influence of clustering and the nature of the interfacial interactions between PDMS matrix and γ–Fe_2O_3 filler.

4.2.2. Hardness. Although hardness (Shore A) values increased with T_c for all samples, they decreased with ϕ_{mnp} at given T_c. Schneider et al. [38] studied the effects of curing temperature on hardness of pure PDMS and also observed a similar behavior. Nobrega et al. [52] studied the effect of different oxide-based nanoparticles types (ZnO, $BaSO_4$, and TiO_2) and suggested that the reason for the reduction could be related to the nature of the nanoparticle as well as the degree of particle-particle interaction within the polymer matrix. These interactions lead to the formation of agglomerates or clusters, which can be detrimental to the mechanical properties of the nanocomposites when their sizes exceed that of the polymer chain [52].

5. Conclusion

This study was performed to investigate and present quantitative data on the effects of curing temperature and nanoparticle volume fraction on the mechanical behavior of PDMS reinforced with γFe_2O_3 nanoparticles. For the temperature range tested (25 – 150°C), Young's modulus increased by over 170%, from 1.36 MPa to 3.71 MPa, and the ultimate tensile strength decreased linearly from 6.48 MPa to 2.93 MPa when nanoparticle volume fraction was varied up to 2 vol. %. Hardness (Shore A) of samples MNP-0, MNP-1, and MNP-2 increased from 42.50 to 52.32, 39.67 to 48.88, and 37.38 to 47.08, respectively, when curing temperature was increased from 25°C to 150°C. On the other hand, the hardness (Shore A) obtained at curing temperatures 25°C, 100°C, and 150°C decreased from 42.50 to 37.38, 46.75 to 42.52, and 52.32 to 47.08, respectively, when the nanoparticle volume fraction was increased from 0 to 2%. In conclusion, we observed a linear relationship between the mechanical properties, and nanoparticle concentration was independent of the curing temperatures tested in this study. Furthermore, the results obtained in this study provide useful background information for the selection of processing parameters for PDMS nanocomposite fabrication.

Data Availability

All data used to support this study are included in the article.

Conflicts of Interest

The authors declare that they have no conflicts of interest.

Acknowledgments

This research was funded by the Building a New Generation of Academics in Africa (BANGA-Africa) project, which is funded by the Carnegie Corporation of New York. Appreciation is also extended to Mrs. Gloria Manu (Materials Science and Engineering Lab) for technical support with the experiments.

References

[1] "SYLGARD 184 silicone elastomer kit," 2019, https://www.dow.com/en-us/pdp.sylgard-184-silicone-elastomer-kit.01064291z.html.

[2] M. Kitsara and J. Ducree, "Integration of functional materials and surface modification for polymeric microfluidic systems," *Journal of Micromechanics and Microengineering*, vol. 23, no. 3, Article ID 033001, 2013.

[3] K. J. Regehr, M. Domenech, J. T. Koepsel et al., "Biological implications of polydimethylsiloxane-based microfluidic cell culture," *Lab on a Chip*, vol. 9, no. 15, pp. 2132–2139, 2009.

[4] H. Becker and L. E. Locascio, "Polymer microfluidic devices," *Talanta*, vol. 56, no. 2, pp. 267–287, 2002.

[5] Y. Xia and G. M. Whitesides, "Soft lithography," *Annual Review of Materials Science*, vol. 28, no. 1, pp. 153–184, 1998.

[6] D. Qin, Y. Xia, and G. M. Whitesides, "Soft lithography for micro- and nanoscale patterning," *Nature Protocols*, vol. 5, no. 3, pp. 491–502, 2010.

[7] T. W. Odom, J. C. Love, D. B. Wolfe, K. E. Paul, and G. M. Whitesides, "Improved pattern transfer in soft lithography using composite stamps," *Langmuir*, vol. 18, no. 13, pp. 5314–5320, 2002.

[8] V. Ozbolat, M. Dey, B. Ayan, A. Povilianskas, M. C. Demirel, and I. T. Ozbolat, "3D printing of PDMS improves its mechanical and cell adhesion properties," *ACS Biomaterials Science & Engineering*, vol. 4, no. 2, pp. 682–693, 2018.

[9] G. Comina, A. Suska, and D. Filippini, "PDMS lab-on-a-chip fabrication using 3D printed templates," *Lab Chip*, vol. 14, no. 2, pp. 424–430, 2014.

[10] T. Fujiwara, I. D. Johnston, M. C. Tracey, and C. K. L. Tan, "Increasing pumping efficiency in a micro throttle pump by enhancing displacement amplification in an elastomeric substrate," *Journal of Micromechanics and Microengineering*, vol. 20, Article ID 065018, 2010.

[11] M. J. Davies, I. D. Johnston, C. K. L. Tan, and M. C. Tracey, "Whole blood pumping with a microthrottle pump," *Biomicrofluidics*, vol. 4, Article ID 044112, 2010.

[12] S. Prauzner-Bechcicki, J. Raczkowska, E. Madej et al., "PDMS substrate stiffness affects the morphology and growth profiles of cancerous prostate and melanoma cells," *Journal of the*

Mechanical Behavior of Biomedical Materials, vol. 41, pp. 13–22, 2015.

[13] R. N. Palchesko, L. Zhang, Y. Sun, and A. W. Feinberg, "Development of polydimethylsiloxane substrates with tunable elastic modulus to study cell mechanobiology in muscle and nerve," *PLoS One*, vol. 7, Article ID e51499, 2012.

[14] I. E. Araci, B. Su, S. R. Quake, and Y. Mandel, "An implantable microfluidic device for self-monitoring of intraocular pressure," *Nature Medicine*, vol. 20, no. 9, pp. 1074–1078, 2014.

[15] T. Jung and S. Yang, "Highly stable liquid metal-based pressure sensor integrated with a microfluidic channel," *Sensors*, vol. 15, no. 5, Article ID 11835, p. 11823, 2015.

[16] M. Liu, J. Sun, and Q. Chen, "Influences of heating temperature on mechanical properties of polydimethylsiloxane," *Sensors and Actuators A: Physical*, vol. 151, no. 1, pp. 42–45, 2009.

[17] I. D. Johnston, D. K. McCluskey, C. K. L. Tan, and M. C. Tracey, "Mechanical characterization of bulk Sylgard 184 for microfluidics and microengineering," *Journal of Micromechanics and Microengineering*, vol. 24, Article ID 035017, 2014.

[18] M.-A. Campeau, A. Lortie, P. Tremblay et al., "Effect of manufacturing and experimental conditions on the mechanical and surface properties of silicone elastomer scaffolds used in endothelial mechanobiological studies," *BioMedical Engineering OnLine*, vol. 16, p. 90, 2017.

[19] M. Vert, Y. Doi, K.-H. Hellwich et al., "Terminology for biorelated polymers and applications (IUPAC recommendations 2012)," *Pure and Applied Chemistry*, vol. 84, no. 2, pp. 377–410, 2012.

[20] B. Pukanszky and E. Fekete, "Adhesion and surface modification," *Mineral Fillers in Thermoplastics*, vol. 139, pp. 109–153, 1999.

[21] K. V. Wong and M. J. Castillo, "Heat transfer mechanisms and clustering in Nanofluids," *Advances in Mechanical Engineering*, vol. 2, Article ID 795478, 2010.

[22] J. S. Bergström and M. C. Boyce, "Mechanical behavior of particle filled elastomers," *Rubber Chem. Technol*, vol. 72, pp. 633–656, 1999.

[23] E. Guth, "Theory of filler reinforcement," *Journal of Applied Physics*, vol. 16, no. 1, pp. 20–25, 1945.

[24] B. Turcsányi, B. Pukánszky, and F. Tüdõs, "Composition dependence of tensile yield stress in filled polymers," *Journal of Materials Science Letters*, vol. 7, no. 2, pp. 160–162, 1988.

[25] L.-W. Jang, J. Lee, M. E. Razu, E. C. Jensen, and J. Kim, "Fabrication of PDMS nanocomposite materials and nanostructures for biomedical nanosystems," *IEEE Transactions on NanoBioscience*, vol. 14, no. 8, pp. 841–849, 2015.

[26] H.-J. Bai, H.-L. Gou, J.-J. Xu, and H.-Y. Chen, "Molding a silver nanoparticle template on polydimethylsiloxane to efficiently capture mammalian cells," *Langmuir*, vol. 26, no. 4, pp. 2924–2929, 2010.

[27] K. Kan-Dapaah, N. Rahbar, and W. Soboyejo, "Implantable magnetic nanocomposites for the localized treatment of breast cancer," *Journal of Applied Physics*, vol. 116, no. 23, Article ID 233505, 2014.

[28] H. SadAbadi, S. Badilescu, M. Packirisamy, and R. Wüthrich, "Integration of gold nanoparticles in PDMS microfluidics for lab-on-a-chip plasmonic biosensing of growth hormones," *Biosensors and Bioelectronics*, vol. 44, pp. 77–84, 2013.

[29] R. Grau-Crespo, A. Y. Al-Baitai, I. Saadoune, and N. H. De Leeuw, "Vacancy ordering and electronic structure of γ-Fe_2O_3 (maghemite): a theoretical investigation," *Journal of Physics: Condensed Matter*, vol. 22, no. 25, Article ID 255401, 2010.

[30] H. Shokrollahi, "A review of the magnetic properties, synthesis methods and applications of maghemite," *Journal of Magnetism and Magnetic Materials*, vol. 426, pp. 74–81, 2017.

[31] A. Ali, H. Zafar, M. Zia et al., "Synthesis, characterization, applications, and challenges of iron oxide nanoparticles," *Nanotechnology, Science and Applications*, vol. 9, pp. 49–67, 2016.

[32] Z. Cao, W. Jiang, X. Ye, and X. Gong, "Preparation of superparamagnetic Fe_3O_4/PMMA nano composites and their magnetorheological characteristics," *Journal of Magnetism and Magnetic Materials*, vol. 320, no. 8, pp. 1499–1502, 2008.

[33] S. Kitano, T. Komatsuzaki, I. Suzuki, M. Nogawa, H. Naito, and S. Tanaka, "Development of a rigidity tunable flexible joint using magneto-rheological compounds-toward a multijoint manipulator for laparoscopic surgery," *Frontiers in Robotics and AI*, vol. 7, p. 59, 2020.

[34] P. S. Antonel, G. Jorge, O. E. Perez, A. Butera, A. G. Leyva, and R. M. Negri, "Magnetic and elastic properties of $CoFe_2O_4$-polydimethylsiloxane magnetically oriented elastomer nanocomposites," *Journal of Applied Physics*, vol. 110, no. 4, Article ID 043920, 2011.

[35] K. Kan-Dapaah, N. Rahbar, A. Tahlil, D. Crosson, N. Yao, and W. Soboyejo, "Mechanical and hyperthermic properties of magnetic nanocomposites for biomedical applications," *Journal of the Mechanical Behavior of Biomedical Materials*, vol. 49, pp. 118–128, 2015.

[36] K. Kan-Dapaah, B. Asimeng, S. K. Kwofie, and A. Yaya, "A plasmonic photo-thermal probe for thermoablation of post-operative breast cancer cells," *Cogent Engineering*, vol. 4, no. 1, Article ID 1331966, 2017.

[37] Y. K. Konku, J. Kutor, A. Yaya, and K. Kan-Dapaah, "Ablation of hepatic tumors through the use of a novel magnetic nanocomposite probe: magnetic characterization and finite element method analysis," *Journal of Nanotechnology*, vol. 2019, no. 9, Article ID 6802125, 2019.

[38] F. Schneider, T. Fellner, J. Wilde, and U. Wallrabe, "Mechanical properties of silicones for MEMS," *Journal of Micromechanics and Microengineering*, vol. 18, no. 6, Article ID 065008, 2008.

[39] P. Scherrer, "Bestimmung der grösse und der inneren struktur von kolloidteilchen mittels röntgenstrahlen," *Mathematisch-Physikalische Klasse*, vol. 2, pp. 98–100, 1918.

[40] C. Becker, H. Krug, and H. Schmidt, "Tailoring of thermomechanical properties of thermoplastic nanocomposites by surface modification of nanoscale silica particles," *MRS Proceedings*, vol. 435, p. 237, 1996.

[41] F. D. Blum, "Silane coupling agents," in *Encyclopedia of Polymer Science and Technology*, J. I. Kroschwitz, Ed., vol. 8, pp. 38–50, John Wiley & Sons, Hoboken, NJ, USA, 2004.

[42] S. Hayashi, Y. Takeuchi, M. Eguchi, T. Iida, and N. Tsubokawa, "Graft polymerization of vinyl monomers initiated by peroxycarbonate groups introduced onto silica surface by Michael addition," *Journal of Applied Polymer Science*, vol. 71, no. 9, pp. 1491–1497, 1999.

[43] M. Z. Rong, M. Q. Zhang, Y. X. Zheng, H. M. Zeng, R. Walter, and K. Friedrich, "Irradiation graft polymerization on nanoinorganic particles: an effective means to design polymer-based nanocomposites," *Journal of Materials Science Letters*, vol. 19, no. 13, pp. 1159–1161, 2000.

[44] C.-L. Wu, H.-C. Lin, J.-S. Hsu, M.-C. Yip, and W. Fang, "Static and dynamic mechanical properties of polydimethylsiloxane/

carbon nanotube nanocomposites," *Thin Solid Films*, vol. 517, no. 17, pp. 4895–4901, 2009.

[45] W. D. J. Callister, *Materials Science and Engineering, An Introduction*, John Wiley & Sons, Inc., New York, NY, USA, 2007.

[46] H. Denver, T. Heiman, E. Martin, A. Gupta, and D. A. Borca-Tasciuc, "Fabrication of polydimethylsiloxane composites with nickel nanoparticle and nanowire fillers and study of their mechanical and magnetic properties," *Journal of Applied Physics*, vol. 106, no. 6, Article ID 064909, 2009.

[47] E. Guth and O. Gold, "On the hydrodynamical theory of the viscosity of suspensions," *Physical Review*, vol. 53, p. 322, 1938.

[48] A. Einstein, "Über die von der molekularkinetischen theorie der wärme geforderte bewegung von in ruhenden flüssigkeiten suspendierten teilchen," *Annalen der Physik*, vol. 322, no. 8, pp. 549–560, 1905.

[49] A. Einstein, *Investigation on Theory of Brownian Motion*, Dover, New York NY, USA, 1956.

[50] S.-Y. Fu, X.-Q. Feng, B. Lauke, and Y.-W. Mai, "Effects of particle size, particle/matrix interface adhesion and particle loading on mechanical properties of particulate-polymer composites," *Composites Part B: Engineering*, vol. 39, no. 6, pp. 933–961, 2008.

[51] T. L. Smith, "Volume changes and dewetting in glass bead-polyvinyl chloride elastomeric composites under large deformations," *Transactions of the Society of Rheology*, vol. 3, no. 1, pp. 113–136, 1959.

[52] A. S. Nobrega, A. M. Andreotti, A. Moreno, M. A. C. Sinhoreti, D. M. dos Santos, and M. C. Goiato, "Influence of adding nanoparticles on the hardness, tear strength, and permanent deformation of facial silicone subjected to accelerated aging," *The Journal of Prosthetic Dentistry*, vol. 116, no. 4, pp. 623–629, 2015.